



THE UNIVERSITY *of* EDINBURGH

Edinburgh Research Explorer

Aerodynamic and Radiative Controls on the Snow Surface Temperature

Citation for published version:

Pomeroy, JW, Essery, R & Helgason, WD 2016, 'Aerodynamic and Radiative Controls on the Snow Surface Temperature', *Journal of Hydrometeorology*. <https://doi.org/10.1175/JHM-D-15-0226.1>

Digital Object Identifier (DOI):

[10.1175/JHM-D-15-0226.1](https://doi.org/10.1175/JHM-D-15-0226.1)

Link:

[Link to publication record in Edinburgh Research Explorer](#)

Document Version:

Peer reviewed version

Published In:

Journal of Hydrometeorology

General rights

Copyright for the publications made accessible via the Edinburgh Research Explorer is retained by the author(s) and / or other copyright owners and it is a condition of accessing these publications that users recognise and abide by the legal requirements associated with these rights.

Take down policy

The University of Edinburgh has made every reasonable effort to ensure that Edinburgh Research Explorer content complies with UK legislation. If you believe that the public display of this file breaches copyright please contact openaccess@ed.ac.uk providing details, and we will remove access to the work immediately and investigate your claim.



Aerodynamic and Radiative Controls on the Snow Surface Temperature

J. W. Pomeroy¹

Centre for Hydrology, University of Saskatchewan
Saskatoon, Saskatchewan, Canada

R. L. H. Essery

School of Geosciences, University of Edinburgh
Edinburgh, Scotland, United Kingdom

W. D. Helgason

Civil and Geological Engineering, University of Saskatchewan,
Saskatoon, Saskatchewan, Canada

¹Corresponding author address: John Pomeroy, Centre for Hydrology, University of Saskatchewan, 117
Science Place, Saskatoon, SK, CANADA, S7N 5C8
Email: john.pomeroy@usask.ca

Abstract

35

36

37 The snow surface temperature (SST) is essential for estimating longwave radiation fluxes
38 from snow. SST can be diagnosed using fine-scale multilayer snow physics models that
39 track changes in snow properties and internal energy, however these models are heavily
40 parameterized, have high predictive uncertainty and require continuous simulation to
41 estimate prognostic state variables. Here, a relatively simple model to estimate SST that
42 is not reliant on prognostic state variables is proposed. The model assumes that the snow
43 surface is poorly connected thermally to the underlying snowpack and largely transparent
44 for most of the shortwave radiation spectrum, such that a snow surface energy balance
45 amongst only sensible heat, latent heat, longwave radiation and near-infrared radiation is
46 possible and is called the Radiative Psychrometric Model (RPM). The RPM modelled
47 SST is sensitive to air temperature, humidity, ventilation and longwave irradiance and is
48 secondarily affected by absorption of near-infrared radiation at the snow surface which
49 was higher where atmospheric deposition of particulates was more likely to be higher.

50 The model was implemented with neutral stability, an implicit windless exchange
51 coefficient, and constant shortwave absorption factors and aerodynamic roughness
52 lengths. It was evaluated against radiative SST measurements from the Canadian Prairies
53 and Rocky Mountains, French Alps and Bolivian Andes. With optimized and global
54 shortwave absorption and aerodynamic roughness length parameters it is shown to
55 accurately predict SST under a wide range of conditions, providing superior predictions
56 when compared to air temperature, dew point or ice bulb calculation approaches.

57

58

59 1. Introduction

60 The snow surface temperature (SST) is an important variable in energy balance
61 calculations of snowpack energetics and as a lower boundary condition for the
62 atmosphere over snow-covered surfaces (King et al., 2008). The SST is defined here as
63 the temperature responsible for longwave exitance and is not the temperature of the
64 uppermost few cm of the snowpack. It forms the basis for calculations of longwave
65 emission from the snowcover and a lower reference condition for calculations of sensible
66 and latent heat flux (Kondo and Yamazaki, 1990; Marks et al., 1992; Fierz et al., 2003).
67 These calculations govern the coupled energy and mass budget equations that determine
68 snow dynamics, particularly the energy state of snow, surface sublimation and snowmelt.
69 Various methods exist to estimate SST, including: the assumption that it is at 0 °C when
70 melting and otherwise related to air temperature when net radiation is positive (Jordan,
71 1991; Marsh and Pomeroy, 1996); modified force-restore techniques (e.g. Luce and
72 Tarboton, 2010); heat conduction equations (e.g. Tarboton and Luce, 1996; Singh and
73 Gan, 2005); dew-point methods (Andreas, 1986; Raleigh et al., 2013); and methods that
74 employ the coupled mass and energy balance equations including radiation to snow
75 (Kondo and Yamazaki, 1990; Jordan, 1991; Lehning et al., 2002; Ellis et al., 2010).
76 Many land surface schemes (LSS) for atmospheric models include explicit SST
77 calculations – these are usually coupled energy and mass balance calculations for an
78 infinitesimal ‘skin’ layer of snow [e.g. CLASS (Canadian Land Surface Scheme) -
79 Verseghy, 1991, 1993; CLM (Community Land Model) – Oleson, 2008; JULES (Joint
80 UK Land Environment Simulator) – Best et al., 2011), though a version of the ISBA
81 (Interaction Soil Biosphere Atmosphere) model uses the force restore method (Douville,

82 1995). Evaluation of LSS performance over snow has suggested that most LSS become
83 too cold over the winter and this could be partly due to an overestimation of longwave
84 energy loss from snowpacks in some of these models (Slater et al., 2001). Energy
85 balance snow models used for hydrology and snow dynamics vary from single layer
86 models such as EBSM (Energy Budget Snowmelt Model - Gray and Landine, 1988) to
87 more physically-detailed layered models such as SNOBAL (Marks et al. 1999, 2008),
88 SNTHERM (Jordan, 1991), CROCUS (Brun, 1989,1992; Vionnet et al., 2012), and
89 SNOWPACK (Bartelt and Lehning, 2002). Marks et al. (2008) have shown that the
90 performance of physically based layered snowmelt models is very sensitive to how the
91 upper model snow layers are parameterized. A recent snow model intercomparison study
92 found that many of the models had significant discrepancies in their longwave exitance
93 when compared to observations (Rutter et al., 2009).

94 What is not always appreciated in process or modelling studies of SST is the
95 strong difference between the temperature at the snow surface and the temperature just
96 below or near the snow surface. A recent study (Helgason and Pomeroy, 2012b)
97 including detailed fine-wire thermocouple measurements of temperatures just below the
98 snow surface (0-10 cm) found that they were strongly related to the 1.5 m air temperature
99 because of convection through porous media – in contrast, radiometrically measured
100 surface temperatures were up to 4°C colder than the snow just below. This is consistent
101 with microwave observations of wet snow under freezing snow surfaces (Koh and
102 Jordan, 1995) and the rapid change in SST upon exposure in a snowpit wall (Schirmer,
103 2014). It is therefore important to define the snow surface temperature as that occurring
104 on the upper boundary of the snowpack; the boundary that is responsible for longwave

105 exitance. Because longwave radiation is not transmitted through snow or water and has a
106 very low reflectance (Dozier and Warren, 1982), this boundary is likely to be exceedingly
107 thin and will lay above the physical layers that can be measured with fine-wire
108 thermocouple thermometry.

109 The wide variety of methods and apparent deficiencies in land surface scheme and
110 snow model estimates of longwave exitance suggest a need to more fully understand the
111 major energy and mass fluxes that control the SST and how these might be reliably
112 calculated outside of full mass and energy balance models. Some methods focus on the
113 radiometric cooling of the snowpack (Marsh and Pomeroy, 1996), some on conduction
114 from the snowpack (Luce and Tarboton, 2010), whilst some focus on the aerodynamic
115 considerations (Andreas, 1986). It would be advantageous for calculating SST if
116 methods could avoid relying on uncertain prognostic state variables such as the internal
117 energy of the snowpack or the albedo of the snowpack. This avoids accumulation of
118 biases in estimating snow surface and internal energy state that are a large source of error
119 in snow models (Essery et al, 2013).

120 The purpose of this paper is to document observations of SST in a wide variety of
121 environments and attempt to relate these observations in a tractable to the main driving
122 aerodynamic and radiative energy fluxes via a simple predictive model with minimal
123 driving variable and parameter requirements. Parameter uncertainty and optimality are
124 examined to derive a robust predictive model of SST. By doing so, the relative
125 importance of aerodynamic and radiative transfer in controlling the SST under various
126 environmental conditions can be diagnosed and the applicability of the model for
127 estimating SST can be evaluated for global applications.

128 2. Theory

129 The longwave exitance, LW_{\uparrow} from a snow surface can be found using the assumption
 130 that it is a near black body from the Stefan Boltzmann formulation,

$$131 \quad LW_{\uparrow} = (1 - \varepsilon)LW_{\downarrow} + \varepsilon\sigma T_s^4, \quad (1)$$

132 where ε is the emissivity in the thermal infrared range (λ from 8 to 12 μm), LW_{\downarrow} the
 133 incoming longwave radiation to the surface, $\sigma = 5.67 \times 10^{-8} \text{ W m}^{-2} \text{ K}^{-4}$ is the Stefan-
 134 Boltzmann constant and T_s is the surface temperature of the snowpack (SST) in K.

135 Dozier and Warren (1982) and Marks and Dozier (1992) showed that ε varies from 0.98
 136 to 0.99 for snow, depending on viewing angle. Hori et al (2006) found both an angular
 137 and a grain size dependency on emissivity, with values above 0.98 for fine, medium, and
 138 most coarse grained snow with exceptional values from 0.90 to 0.98 for some sun crust
 139 snow where specular reflection of thermal infrared radiation was observed. In practice,
 140 many calculations (e.g. Best et al., 2011) assume that $\varepsilon = 1$. The critical variable to
 141 estimate in Eq. (1) is the SST, T_s , which is further defined here as the longwave radiant
 142 temperature of snow to distinguish it from the temperatures of sub-surface layers that
 143 may not correspond to the thermal radiating surface (Helgason and Pomeroy, 2012b).
 144 Many procedures to estimate SST (Armstrong and Brun, 2008) employ a form of the
 145 energy balance, where the SST is found as the result of an iterative or linearized solution
 146 to the energy equation for snow,

$$147 \quad SW^* + LW^*(T_s) + LE(T_s) + H(T_s) + G = M + \frac{dU}{dt}, \quad (2)$$

148 where SW^* is net shortwave radiation, LW^* is net longwave radiation, LE is the latent
149 heat flux due to sublimation, H is the sensible heat flux to the snow, G is the ground heat
150 flux M , is the latent heat flux due to melting and U is internal energy state of the snow.
151 The net longwave, sensible and latent heat flux terms are a function of the SST in regard
152 to their surface reference conditions. The disposition of energy between M and internal
153 energy change is also controlled by snow temperatures including the SST. However,
154 solving for the SST from an energy budget such as Eq. (2) presumes that i) the SST is
155 well-coupled to that of the underlying snowpack, and ii) all snowpack mass and energy
156 exchanges with the atmosphere occur exactly at the surface. Some procedures try to
157 compensate for this by calculating the energy state of multiple layers in a snowpack (e.g.
158 Jordon, 1991) or separating a surface layer calculation from the bulk snowpack
159 temperature calculation using a heat conduction term (e.g. Versegby, 1993). Kondo and
160 Yamazaki (1990) remove the shortwave component from the energy balance of the
161 surface layer, assuming complete reflection and transmission of shortwave radiation
162 through the surface and absorption in interior snowpack layers. These compensations still
163 need to estimate a fairly comprehensive set of energy exchange calculations at the
164 surface, as well as the snow thermal conductivity, ground heat flux and an internal
165 snowpack temperature gradient. Cumulative errors in estimating internal snow energy
166 state can cause large errors in the radiative balance and turbulent exchanges with snow
167 (Pomeroy et al., 1998; Helgason and Pomeroy, 2012b).

168 A photograph taken of an upper layer of a natural late-winter snowpack in Yukon,
169 Canada shows a “skin” layer at the surface that appears to be not well structurally
170 connected to the rest of the snowpack (**Fig. 1**). Individual snow crystals at the top of the

171 snowpack are well exposed to the atmosphere and tenuously connected to the rest of the
 172 snowpack by slender bonds. This is a typical condition for snow; snow surfaces are often
 173 composed of a persistent surface hoar with a very sparse bond structure connecting these
 174 crystals to the ice matrix below (Hachikubo and Akitaya, 1997; Stössel et al., 2010). In
 175 this layer the tenuous bonds that connect the top surface crystals to the rest of the
 176 snowpack will conduct very little heat due to their low thermal conductivity and will have
 177 a very small heat capacity as shown by the measurements of Helgason and Pomeroy
 178 (2012b). This structure suggests that the surface may be poorly coupled by heat
 179 conduction with the rest of the snowpack and therefore the usefulness of Eq. (2) in
 180 estimating T_s needs to be reassessed. As liquid water and ice are exceedingly poor
 181 transmitters of thermal infrared radiation, it can be presumed with confidence that only
 182 the outer surface layer of the upper layer of crystals of this snowpack is active in emitting
 183 longwave radiation. Further one may assume that the outer surface layer reflects or
 184 transmits most of the incident visible shortwave radiation (Kondo and Yamazaki, 1990),
 185 but absorbs some of the near infrared (NIR) shortwave radiation, depending on grain size
 186 (Wiscombe & Warren, 1980) mineral dust, biological materials and black organic carbon
 187 (Dang et al., 2015). This system is analogous to an aspirated ice bulb with longwave and
 188 NIR radiative inputs. From these considerations, a greatly simplified model of the energy
 189 balance in relation to the snow surface temperature can be proposed as

$$190 \quad \text{NIR}^* + \text{LW}^*(T_s) + \text{LE}(T_s) + H(T_s) = 0. \quad (3)$$

191 Here it is understood that the NIR^* term is not normally measured and that it can be
 192 found as a function of net shortwave irradiance, SW^* , at the snow surface. This radiative-
 193 psychrometric model (RPM) of SST has certain operational advantages over other

194 methods in that it: (1) does not require information on the energy state of the snowpack or
 195 substrate; and (2) requires only standard atmospheric information (wind speed,
 196 temperature, humidity) and incoming radiation. The terms in the RPM are parameterized
 197 as

$$198 \quad f_{abs} SW_{\downarrow} + \varepsilon (LW_{\downarrow} - \sigma T_s^4) = \frac{\rho}{r_a} \left\{ c_p (T_a - T_s) + L [Q_a - Q_{sat}(T_s, P_s)] \right\}, \quad (4)$$

199 where f_{abs} is a surface shortwave radiation absorption factor to help estimate NIR* from
 200 incoming shortwave radiation measurement (if 1 then all radiation is absorbed, if 0 then
 201 no radiation is absorbed), ε is the emissivity of snow, taken as 0.985, ρ is the air density
 202 (kg m^{-3}), r_a is the aerodynamic resistance (s m^{-1}), $c_p = 1005 \text{ J kg}^{-1} \text{ K}^{-1}$ is the specific heat
 203 capacity of air, $L = 2.835 \times 10^{-6} \text{ J kg}^{-1}$ is the latent heat of sublimation and Q_a is the
 204 specific humidity of the air. $Q_{sat}(T_s, P_s)$ is the saturation specific humidity at snow surface
 205 temperature T_s and surface air pressure P_s , which can be approximated by the Buck
 206 (1981) formula,

$$207 \quad Q_{sat} = \frac{3.8}{P_s} \exp\left(\frac{22.452T}{272.55 + T}\right), \quad (5)$$

208 for temperature in $^{\circ}\text{C}$ and pressure in hPa. For application to the snow surface, $T = T_s$.
 209 Neglecting corrections for atmospheric stability near to the surface (Andreas, 1986), the
 210 aerodynamic resistance can be found as

$$211 \quad r_a = \frac{k^2}{U} \ln\left(\frac{z_T}{z_0}\right) \ln\left(\frac{z_U}{z_0}\right), \quad (6)$$

212 where $k = 0.4$ is the von Kármán constant, U is the wind speed (m s^{-1}) at height z_U (m),
 213 z_T is the measurement height of the air temperature, T_a , and z_0 is the aerodynamic
 214 roughness length for snow (m). For simplicity, aerodynamic exchange in RPM does not

215 consider stability corrections and anemometer stall speeds (assumed 0.1 m s^{-1}) are the
 216 lowest wind speeds used to drive Eq. (6). The lack of stability corrections is supported
 217 by the uncertainty in stability corrections found from careful field tests in mountains
 218 (Stossel et al., 2010; Martin and Lejeune, 1998; Helgason and Pomeroy, 2012a) and level
 219 sites (Helgason and Pomeroy, 2012b).

220 The left hand side of Eq. (4) is radiative and the right hand side is aerodynamic.
 221 Under conditions of low ventilation (high r_a) it can be presumed that the radiative terms
 222 will dominate calculation of the snow surface temperature and under high ventilation
 223 (low r_a) aerodynamic terms will become more important. The relative contribution of
 224 radiative and aerodynamic terms can be described by apportioning the SST between a
 225 radiative equilibrium temperature, T_{req} , and an aerodynamic equilibrium temperature,
 226 T_{aeq} . The radiative equilibrium temperature can be found using the Stephan-Boltzmann
 227 equation and the assumption that the SST is determined completely by radiation balance,
 228 giving

$$229 \quad T_{req} = \left[\frac{f_{abs} SW_{\downarrow} + \epsilon LW_{\downarrow}}{\epsilon \sigma} \right]^{1/4}. \quad (7)$$

230 The aerodynamic equilibrium temperature for full ventilation (the ice bulb temperature)
 231 can be found for the condition $r_a = 0$ as

$$232 \quad T_{aeq} = T_a + \frac{L}{c_p} \left[Q_a - Q_{sat}(T_{aeq}, P_s) \right]. \quad (8)$$

233 Note that this is an implicit equation that requires an iterative solution for T_{aeq} .

234 Apportionment of the SST between radiative and aerodynamic equilibria is governed by
 235 the degree of ventilation, such that

236
$$T_s = (1 - f_v)T_{req} + f_v T_{aeq}, \quad (9)$$

237 and f_v is a ventilation factor varying from 0 for an aerodynamically decoupled surface
 238 ($r_a = \infty$) to 1 for a perfectly ventilated surface ($r_a = 0$). Rearranging Eq. (9) to solve for
 239 f_v in terms of aerodynamic equilibrium, radiative equilibrium and SST gives,

240
$$f_v = \frac{T_s - T_{req}}{T_{aeq} - T_{req}}, \quad (10)$$

241 which shows that as the SST approaches radiative equilibrium and/or the difference
 242 between the aerodynamic and radiative equilibrium temperatures increases, then f_v
 243 approaches zero.

244 The RPM requires knowledge of air temperature, humidity, wind speed, incoming
 245 longwave and shortwave radiation, aerodynamic roughness and atmospheric pressure
 246 (which can be measured or found from site elevation). Its parameters are snow
 247 aerodynamic roughness length and shortwave absorption factor. Aerodynamic roughness
 248 can be measured or estimated from published values. Estimation of the shortwave
 249 absorption factor at the surface requires information on the spectral distribution of
 250 shortwave radiation, the spectral albedo of the snow surface, angular reflectance and the
 251 extinction of NIR in snow. All of these factors vary in complex ways; the spectral
 252 distribution of radiation with atmospheric conditions and multiple reflections by
 253 vegetation and terrain, the spectral albedo of snow with surface grain size, contaminants
 254 and liquid water content and radiation extinction with snow structure and contamination
 255 (Pomeroy and Brun, 2001). It is possible to estimate snow radiative absorption using the
 256 calculations described by Warren and Wiscombe (1980) with recent adjustments for
 257 contaminants (Dang et al., 2015), but such estimates will depend on uncertain

258 assumptions of surface layer thickness, dust, black carbon or organic matter
259 contamination, grain size, wetness and on the site specific spectral irradiance. This factor
260 is expected to be small because NIR is less than half of shortwave radiation and not all
261 NIR is extinguished at the snow surface. As such it should be less than $(1 - \text{albedo})$ and
262 so should be less than 0.1 for fresh, clean snow and less than 0.3 for dirty, wet snow.

263 3. Sensitivity Analysis

264 The RPM was investigated initially with a sensitivity analysis of its driving variables
265 using fixed parameters in order to demonstrate how wind speed influences the ventilation
266 factor and how temperature, humidity, wind speed and radiation influence the snow
267 surface temperature. **Fig. 2** shows that the ventilation factor, f_v , increases initially rapidly
268 from 0 as wind speed, U , increases and approaches 1 asymptotically as wind speeds
269 become high. Wind speed, temperature and humidity for this example are from a
270 reference height of 2 m above the snow surface and relative humidity is with respect to
271 ice. Example conditions are; relative humidity = 80%, incoming longwave radiation =
272 250 W m^{-2} and wind speed = 2 m s^{-1} . The rapid rate of change in f_v for low wind speeds
273 shows that only a moderate degree of ventilation is required for aerodynamic equilibrium
274 conditions to dominate SST; the effect of low wind speed is to decouple the surface
275 temperature from aerodynamic effects and so it becomes dominated by radiation. **Fig. 3**
276 shows T_s , T_{aeq} , and T_{req} similarly estimated using the RPM as a function of wind speed,
277 relative humidity, and incoming longwave radiation. Figure 3a shows the strong
278 influence of air temperature on the aerodynamic equilibrium temperature but not on the
279 radiative equilibrium. There is a nexus where T_{req} , T_s and T_{aeq} are equal – for air

280 temperatures below that of the nexus T_s is elevated above the air temperature; for air
281 temperatures greater than the nexus, T_s is depressed relative to the air temperature
282 reflecting contributions from both aerodynamic and radiative components of the energy
283 balance in controlling the SST. The nexus point and relative T_s elevation and depression
284 are specific to the example conditions. As the relative humidity and wind speed increase,
285 T_s and T_{aeq} rise towards T_a (Fig. 3b, d) and, consistent with Fig 2, as wind speed
286 increases, T_s moves closer to the aerodynamic equilibrium and further from the radiative
287 equilibrium. As irradiance increases (Fig. 3c), T_s and T_{req} increase until they surpass the
288 constant aerodynamic equilibrium temperature, crossing at a nexus where T_{req} , T_s and T_{aeq}
289 are equal. For low irradiance (below the nexus), T_{aeq} is greater than T_{req} and increasing
290 the wind speed causes T_s to increase. For high irradiance (above the nexus), T_{req} is
291 greater than T_{aeq} and increasing the wind speed causes T_s to decrease. The sensitivity
292 analysis shows that solutions which consider both radiative and aerodynamic factors are
293 necessary to calculate the snow surface temperature for a wide range of environmental
294 conditions.

295 4. Observations

296 Observations of driving meteorology and snow surface temperatures to parameterize and
297 test the RPM were taken at mountain pasture, lake and glacier and prairie pasture and
298 agricultural field sites in North and South America and obtained from data carefully
299 collected by Météo-France in a large forest clearing mountain site in Europe. Data
300 collection at the Americas sites was during periods of frequent site visits, which included
301 frequent radiometer checking and cleaning. Kipp and Zonen (KZ) CNR1 radiometers
302 were heated to reduce frost and snow accumulation. Data collection at the Météo-France

303 site involved hourly cleaning of radiometers to ensure high quality measurements over a
304 long time period. All sites except for the French site had uniform, level fetches of at least
305 100 m with short or non-existent vegetation. Site locations and photographs are shown in
306 **Fig. 4** and site descriptions follow. **Table 1** lists instrumentation used to measure snow
307 surface temperature and the driving meteorological variables.

308

309 **Pomeroy Acreage**, Saskatchewan, Canada (52°02' N, 106°38' W, 508 m.a.s.l.)

310 Measurements were taken every 15 minutes over an undulating snow-covered
311 prairie grassland with greater than 100 m of open fetch in central Saskatchewan, Canada,
312 6 km south of the city of Saskatoon from 15 February to 19 March 2004. The region
313 sustains a sub-humid continental climate with cold, dry winters. The site was snow-
314 covered with at least 25 cm snow depth throughout the experiment but a small amount of
315 grass was exposed above the snow surface.

316

317 **Kernen Farm**, Saskatchewan, Canada (52.09°N, 106.31°W, 512 m.a.s.l.)

318 Measurements were taken every 15 minutes as part of a study published by
319 Helgason and Pomeroy (2012b) over a level cultivated fallow field with greater than 100
320 m of fetch, 2.5 km east of the city of Saskatoon from 23 Jan to 2 March 2007. Climate is
321 similar to the Pomeroy Acreage. The site was snow-covered throughout the experiment
322 with a depth of approximately 42 cm.

323

324 **Mud Lake**, Alberta, Canada (50° 47'N, 115° 18'W, 1896 m.a.s.l.)

325 Measurements were taken every 30 minutes on a frozen lake surface with greater
326 than 100 m of fetch in the Spray Valley, Canadian Rockies from 24-30 January 2006.
327 This is a cold continental site with deep, even snow covering the lake with at least 80 cm
328 depth. The site experiences significant shading from surrounding mountains in January.

329

330 **Zongo Glacier**, Bolivia (16°15'S, 68°10'W, 5150 m.a.s.l.)

331 Measurements were taken every 30 minutes from 8-16 August 2004 as part of a
332 joint France-Canada study at a site with more than 100 m of fetch described by Sicart et
333 al. (2005) on a flat, snow-covered lower lobe of the Zongo Glacier, Huayna Potosi
334 Massif, Cordillera Real, Bolivia. Climate is typical of tropical glaciers and the austral
335 winter was cool with occasional snowfall. The surface was primarily covered with a
336 shallow snowcover, but glacier ice patches were exposed during the measurement period.

337

338 **Col de Porte**, France (45.30°N, 5.77°E, 1325 m.a.s.l.)

339 Measurements as part of a study published by Morin et al. (2012) were taken
340 every 60 minutes by Météo-France over a mown grass surface in a forest clearing in a
341 mountain pass, Chartreuse mountain range, French Alps from 1993 to 2011. The forest
342 edge on three sides was initially 25 to 50 m from the instruments and a large building was
343 50 m away on the fourth side. Forest clearing after 1999 left forest on two sides and the
344 large building on the other. Shading by trees and mountains occurs at this site in winter.
345 The climate is temperate humid continental with substantial snowfall and mild winter
346 temperatures. Snow depth exceeds 50 cm for much of the winter and shallow snow
347 periods were excluded from our analysis.

348

349 **Hay Meadow**, Marmot Creek, Alberta (50°56'N, 115°08'W, 1436 m.a.s.l.)

350 Measurements as part of a study by Helgason and Pomeroy (2005, 2012a) were
351 taken every 30 minutes from a large, gently sloping, grass covered clearing with at least
352 60 m fetch in a mixed-wood forest in Marmot Creek Research Basin, Kananaskis Valley,
353 Canadian Rocky Mountains from 13 February to 5 March 2005. The site was snow-
354 covered throughout the experiment with a depth greater than 15 cm, but a small amount
355 of sparse grass was exposed above the snowpack.

356 5. Analysis

357 The RPM was run with the time step available from the dataset (15 to 60 min.) over the
358 six sites, five of them with observations available for one snow season and one site for 18
359 seasons, depending on data availability. To investigate sensitivity to model parameters,
360 the model was run 1681 times for each of the sites with 41 values of the surface
361 shortwave radiation absorption factor in linear increments from 0 to 1 and 41 values of
362 the aerodynamic roughness length in logarithmic increments from 10^{-4} to 1 m. A 35 day
363 calibration and demonstration season (January 2006) was chosen from the large Col de
364 Porte dataset. **Fig. 5** shows contour plots of root mean square (rms) differences between
365 simulated and measured surface temperatures from these runs. For each site, a unique
366 parameter combination that minimizes the rms error without equifinality was found; these
367 parameter values, along with minimum rms errors and corresponding average errors
368 (bias) in surface temperature, are given in **Table 2**. The optimized shortwave absorption
369 factor was small (<15%) for all sites, and very small (<5%) to zero at two sites. The
370 smaller absorption factors occurred at the higher latitude mid-winter sites in Canada

371 where there were no local sources of dust or organic material (Hay Meadow sometimes
372 had some sparse exposed grass above and on the snow and was near a gravel road source
373 of dust), suggesting that NIR absorption effects on SST are primarily important for
374 conditions where dust, organic material and black carbon deposition may occur. Dust
375 deposition is more common on snow in temperate and tropical mountain environments
376 where there are nearby geological sources. The optimized roughness length was quite
377 variable between sites, varying from 0.001 m for Mud Lake to 0.063 m for Col de Porte.
378 The optimal roughness length for the four flat, long fetch sites in the Canadian prairies
379 and mountains was small, averaging 0.004 m, whilst higher roughness lengths on the
380 Zongo Glacier (0.032 m) and Col de Porte (0.063) may reflect local boundary layer
381 characteristics on a rough glacier and near a forest edge respectively.

382 **Fig. 6** shows RPM simulations and observations of SST at single seasons for the
383 six sites with the optimal parameters (Table 2) for each site. The figure illustrates the
384 generally good fit (Table 2) of the optimized RPM to observations for a wide range of
385 environments (prairies to mountains to glaciers) and SST (0 to -40 °C). The same model
386 runs can be used to examine the behavior of the ventilation factor, f_v , at the various sites
387 (**Fig. 7**). The prairie sites were usually well ventilated with high f_v except for periods
388 when strong inversions formed under relatively calm winds – these were often at night
389 but substantial multi-day well-ventilated periods with high f_v were common both day
390 and night. The non-glaciated mountain sites in Canada, both valley bottom sites, showed
391 lower overall ventilation factors than in the prairies, and stronger diurnal fluctuations
392 consisting of high f_v during the day and low values at night. Valley bottom inversions
393 are common after sunset in this environment and so likely explain this behavior. The Col

394 de Porte site is partly surrounded by forest and its highly variable but generally low f_v is
395 likely associated with its variable fetch, and forest and complex terrain influence on wind
396 flow. The Zongo Glacier site experienced consistently high ventilation factors which are
397 due to its drainage winds rather than inversions at night and excellent wind exposure on a
398 high mountain. Overall, the range of f_v from 0.95 to 0.25 shows that both radiation and
399 ventilation are important in controlling the SST and should be included in a SST model.
400 Note that wind speeds were limited to a minimum value of 0.1 to avoid anemometer
401 stalling. This amounts to an implicit windless exchange coefficient for these model tests
402 and keeps the ventilation factor from reaching very small values.

403 To evaluate potential model performance with global parameters and the necessity
404 of using shortwave radiation to drive the RPM the model was run with 10% and 0%
405 shortwave radiation absorption, for smooth (0.003 m) and rough (0.03 m) aerodynamic
406 roughness lengths for the complete dataset at all sites. The results are plotted as observed
407 versus modelled data in **Fig. 8** and the statistics for these simulations are listed in **Table**
408 **3**. The best global parameter simulations based on rms were for Mud Lake, Kernan Farm,
409 Pomeroy Acreage, and Zongo Glacier – all sites with long open fetch, good wind
410 exposure and rms errors < 1.3 K. The best simulations based on bias were Pomeroy
411 Acreage, Col de Porte and Zongo. The poorest simulations based on rms and/or bias
412 were for Hay Meadow and Col de Porte which had forests nearby and rms errors ranging
413 from 2.3 to 3.5 K for the best set of global parameters. The only site with notably larger
414 errors than the others is Hay Meadow. This site has an extremely gusty turbulent regime
415 (Helgason and Pomeroy, 2005) and sometimes had exposed grass above the snow. The
416 gustiness of the site might have degraded the aerodynamic calculations and the exposed

417 grass may have affected surface temperature measurements. The parameter combination
418 of smooth with 10% shortwave absorption provided the best simulations (rms) for the
419 relatively level prairie and Hay Meadow mountain valley bottom sites whilst the rough
420 and 10% shortwave absorption combination was optimal for the complex terrain sites:
421 Col de Porte and Zongo Glacier. For the Mud Lake simulations (frozen lake snowpack,
422 very clean snow, low insolation period in mid-winter) the optimal parameters were for
423 zero shortwave absorption and a smooth aerodynamic roughness reflecting its extremely
424 smooth and high albedo condition. There was no benefit to using shortwave radiation
425 data to run the model for Mud Lake and little benefit at the prairie and mountain valley
426 sites in Canada as small differences in bias and rms show, however rms errors increased
427 appreciably by from 0.85 to 1.66 K, when radiation absorption was not included at the
428 tropical and temperate mountain sites in Bolivia and France where both high insolation
429 and contamination of snow are more probable. It is clear that there is no one global
430 parameter set but that site information can be used to choose parameters from the set
431 shown in bold in Table 3 and demonstrated in Fig. 8. High latitude sites where
432 snowpacks are normally clean with relatively little dust deposition do not require
433 consideration of shortwave absorption, whilst lower latitude sites do. Sites on frozen
434 lakes, open valley bottoms and on prairie are best served with a small aerodynamic
435 roughness length, whilst those on glaciers and near forests and complex terrain should
436 use a larger length. It is likely a dynamical model of shortwave absorption would provide
437 improved values for the absorption parameter and its seasonal evolution but at the
438 expense of a substantial increase in RPM model complexity.

439 Any new model needs a test of its transferability to datasets not involved in its
440 optimization or selection of global parameters. To test the RPM, the full 18 year dataset
441 from Col de Porte was used with the global parameter set for a rough aerodynamic
442 surface with 10% shortwave absorption (Table 3) and results are shown in **Fig. 9**. The
443 rms error of 2.56 K and bias of -0.81 K are similar to the January 2006 data shown in
444 Table 3 for the same global parameter set, suggesting model predictive stability despite
445 climate variability and changes in site conditions and instrumentation over 18 years.

446 Methods to estimate the SST that use the air temperature, dew point temperature
447 or ice bulb temperature (e.g. Raleigh et al., 2013) are attractive in that they only require
448 information on atmospheric temperature and humidity and so have a requirement for
449 fewer driving variables and parameters than the RPM. Unfortunately these methods lack
450 a physical basis to predict SST and so may not be able to accurately estimate it. To
451 evaluate how well these methods could predict the SST over this dataset, their outputs
452 were compared to observations and the results shown in **Table 4**. The RPM more
453 accurately estimated SST than any of these approaches with rms improvements ranging
454 from 1.15 to 6.33 K. The more accurate of the simple methods were the ice bulb and dew
455 point approaches with rms difference with RPM of only 2.53 and 2.67 K respectively.
456 Errors from assuming the SST was equal to the air temperature were large and the RPM
457 improved these simulations by an rms change of 4.19 K.

458 6. Conclusions

459 The SST is the critically important upper boundary condition for the snowpack and lower
460 boundary condition for the atmosphere and so of great interest to snow scientists,
461 hydrologists and atmospheric scientists. Various methods have been used in snow, land

462 surface and hydrological models to estimate SST and principally they include air
463 temperature, force-restore, heat conduction, dew point, ice bulb, and coupled energy and
464 mass balance calculations. The physically based coupled energy and mass balance
465 methods require a greater number of driving variables and parameters and so have larger
466 uncertainty due to these inputs than do the other methods despite their physical
467 correctness.

468 In an effort to reconcile model complexity, uncertainty, physical correctness and
469 simplicity to create a robust model for estimating SST, the primary driving processes that
470 influence snow surface energetics were identified as aerodynamic (sensible and latent
471 heat transfer) and radiative (thermal and near infrared radiation). A new SST model, the
472 radiative-psychrometric model (RPM) was devised based on this understanding and
473 written so that the radiative and aerodynamic factors controlling SST could be clearly
474 identified. The RPM was tested against careful SST measurements at six sites in North
475 America, South America and Europe that span prairie, mountain, frozen lake and glacier
476 surfaces with various wind exposures and fetch characteristics and was found to perform
477 very well in estimating the SST with optimized parameters for shortwave radiation
478 absorption and aerodynamic roughness length. Global parameters for shortwave
479 absorption and roughness length were identified and applied based on a site
480 classification. High latitude sites with clean snow remote from sources of dust and
481 pollution do not need to consider shortwave absorption in RPM, whilst lower and middle
482 latitude sites do that are proximal to particulate sources do. Sites on frozen lakes, open
483 valley bottoms and on prairie are best served with a small aerodynamic roughness length,
484 whilst those on glaciers and near forests and complex terrain should use a larger length.

485 A test of the RPM with site-selected global parameters for a longer time span at Col de
486 Porte showed good temporal transferability. A comparison of the RPM with recently
487 proposed SST estimation methods shows that the RPM provides superior predictions of
488 SST when compared to air temperature, dew point or ice bulb calculation approaches.

489 7. Acknowledgements

490 The authors would like to acknowledge funding from NSERC, NERC, CFI, CFCAS,
491 Canada Research Chairs, Global Institute for Water Security, Alberta Agriculture and
492 Forestry, and IRD France. The assistance of many students and staff of the Centre for
493 Hydrology over the years was essential to high quality data collection. Data provided by
494 IRD France from Dr. J.E. Sicart and Météo-France from Dr. S. Morin is gratefully
495 acknowledged.

496

497 **References**

498 Andreas, E. L., 1986: A new method of measuring the snow-surface temperature. *Cold*
499 *Reg. Sci. Technol.*, **12**, 139–156, doi:10.1016/0165-232X(86)90029-7.

500

501 Andreas, E. L., 1987: A theory for the scalar roughness and the scalar transfer
502 coefficients over snow and sea ice. *Boundary-Layer Meteorol.*, **38**, 159–184, doi:
503 10.1007/BF00121562.

504

505 Armstrong, R. L., and E. Brun, 2008: *Snow and climate: physical processes, surface*
506 *energy exchange and modeling*. Cambridge University Press. 222 p.

507

508 Bartelt, P., and M. Lehning, 2002: A physical SNOWPACK model for the Swiss
509 avalanche warning Part I: numerical model. *Cold Reg. Sci. Technol.*, **35**, 123–145,
510 doi:10.1016/S0165-232X(02)00074-5.

511

512 Best, M. J., and Coauthors, 2011: The Joint UK Land Environment Simulator (JULES),
513 model description. Part 1: Energy and water fluxes. *Geosci. Model Dev.*, **4**, 677–699,
514 doi:10.5194/gmdd-4-641-2011.

515

516 Brun, E., E. Martin, V. Simon, C. Gendre, and C. Coleau, 1989: An energy and mass
517 balance model of snow cover suitable for operational avalanche forecasting. *Journal of*
518 *Glaciology*, **35**, 333-342.

519

520 Brun, E., P. David, M. Sudul, and G. Brunot, 1992: A numerical model to simulate snow-
521 cover stratigraphy for operational avalanche forecasting. *J. Glaciol.*, **38**, 13–22.

522

523 Buck, A. L., 1981: New Equations for computing vapor pressure and enhancement factor.
524 *J. Appl. Meteorol.*, **20**, 1527–1532, doi:10.1175/1520-
525 0450(1981)020<1527:NEFCVP>2.0.CO;2.

526

527 Dang, C., R. E. Brandt, and S. G. Warren, 2015: Parameterizations for narrowband and
528 broadband albedo of pure snow and snow containing mineral dust and black carbon. *J.*
529 *Geophys. Res. Atmos.*, **120**, doi:10.1002/2014JD022646.

530

531 Douville, H., J. Royer, and J. Mahfouf, 1995: A new snow parameterization for the
532 Meteo-France climate model. *Clim. Dyn.*, **35**, 21–35, doi:10.1007/BF00208760.

533

534 Dozier, J., and S. G. Warren, 1982: Effect of viewing angle on the infrared brightness
535 temperature of snow. *Water Resour. Res.*, **18**, 1424–1434,
536 doi:10.1029/WR018i005p01424.

537

538 Ellis, C. R., J. W. Pomeroy, T. Brown, and J. MacDonald, 2010: Simulation of snow
539 accumulation and melt in needleleaf forest environments. *Hydrol. Earth Syst. Sci.*, **14**,
540 925–940, doi:10.5194/hess-14-925-2010.

541

542 Essery, R., S. Morin, Y. Lejeune, and C. B. Ménard, 2013: A comparison of 1701 snow
543 models using observations from an alpine site. *Adv. Water Resour.*, **55**, 131–148,
544 doi:10.1016/j.advwatres.2012.07.013.

545

546 Fierz, C., P. Riber, E. E. Adams, A. R. Curran, P. M. B. Föhn, M. Lehning, and C. Plüss,
547 2003: Evaluation of snow-surface energy balance models in alpine terrain. *J. Hydrol.*,
548 **282**, 76–94, doi:10.1016/S0022-1694(03)00255-5.

549

550 Gray, D. M., and P. G. Landine, 1988: An energy-budget snowmelt model for the
551 Canadian Prairies. *Can. J. Earth Sci.*, **25**, 1292–1303, doi:10.1139/e88-124.

552

- 553 Hachikubo, A. and E. Akitaya. 1997: Effect of wind on surface hoar growth on snow. *J.*
554 *Geophys. Res.*, **102 D4**, 4367-4373
555
- 556 Helgason, W. D., and J. W. Pomeroy, 2005: Uncertainties in Estimating Turbulent Fluxes
557 to Melting Snow in a Mountain Clearing. *62nd Eastern Snow Conference*, Waterloo,
558 129–142.
559
- 560 ———, and J. W. Pomeroy, 2012a: Characteristics of the near-surface boundary layer
561 within a mountain valley during winter. *J. Appl. Meteorol. Climatol.*, **51**, 583–597,
562 doi:10.1175/JAMC-D-11-058.1.
563
- 564 ———, and J. Pomeroy, 2012b: Problems closing the energy balance over a homogeneous
565 snow cover during midwinter. *J. Hydrometeorol.*, **13**, 557–572, doi:10.1175/JHM-D-11-
566 0135.1.
567
- 568 Hori, M., and Coauthors, 2006: In-situ measured spectral directional emissivity of snow
569 and ice in the 8–14 μm atmospheric window. *Remote Sens. Environ.*, **100**, 486–502,
570 doi:10.1016/j.rse.2005.11.001.
571
- 572 Jordan, R. E., 1991: A One-Dimensional Temperature Model for a Snow Cover. CRREL
573 Special Report 91-16, 49 pp.
574

- 575 King, J., Pomeroy, J.W., Gray, D.M., Fierz, C., Föhn, P. and Coauthors, 2008: Snow-
576 atmosphere energy and mass balance. *Snow and climate: physical processes, surface*
577 *energy exchange and modelling*, Cambridge University Press, 70-124.
578
- 579 Koh, G., and R. Jordan, 1995: Sub-surface melting in a seasonal snow cover. *J. Glaciol.*,
580 **41**, 474–482.
581
- 582 Kondo, J., and T. Yamazaki, 1990: A Prediction model for snowmelt, snow surface-
583 temperature and freezing depth using a heat-balance method. *J. Appl. Meteorol.*, **29**, 375–
584 384.
585
- 586 Lehning, M., P. Bartelt, R. L. Brown, and C. Fierz, 2002: A physical SNOWPACK
587 model for the Swiss avalanche warning: Part III: Meteorological forcing, thin layer
588 formation and evaluation. *Cold Reg. Sci. Technol.*, **35**(3), 169–184.
589
- 590 Luce, C. H., and D. G. Tarboton, 2010: Evaluation of alternative formulae for calculation
591 of surface temperature in snowmelt models using frequency analysis of temperature
592 observations. *Hydrol. Earth Syst. Sci.*, **14**, 535–543, doi:10.5194/hess-14-535-2010.
593
- 594 Marks, D., and J. Dozier, 1992: Climate and energy exchange at the snow surface in the
595 Alpine Region of the Sierra Nevada: 2. Snow cover energy balance. *Water Resour. Res.*,
596 **28**, 3043–3054, doi:10.1029/92WR01483.
597

- 598 ———, J. Domingo, D. Susong, T. Link, and D. Garen, 1999: A spatially distributed
599 energy balance snowmelt model for application in mountain basins. *Hydrol. Process.*, **13**,
600 1935–1959, doi:10.1002/(SICI)1099-1085(199909)13:12/13<1935::AID-
601 HYP868>3.0.CO;2-C.
- 602
- 603 ———, A. Winstral, G. Flerchinger, M. Reba, J. Pomeroy, T. Link, and K. Elder, 2008:
604 Comparing simulated and measured sensible and latent heat fluxes over snow under a
605 pine canopy to improve an energy balance snowmelt model. *J. Hydrometeorol.*, **9**, 1506–
606 1522, doi:10.1175/2008JHM874.1.
- 607
- 608 Marsh, P., and J. W. Pomeroy, 1996: Meltwater fluxes at an arctic forest-tundra site.
609 *Hydrol. Process.*, **10**, 1383–1400, doi:10.1002/(SICI)1099-
610 1085(199610)10:10<1383::AID-HYP468>3.0.CO;2-W.
- 611
- 612 Martin, E., and Y. Lejeune, 1998: Turbulent fluxes above the snow surface. *Ann.*
613 *Glaciol.*, **26**, 179–183.
- 614
- 615 Morin, S., Y. Lejeune, B. Lesaffre, J.-M. Panel, D. Poncet, P. David, and M. Sudul, 2012:
616 A 18-yr long (1993–2011) snow and meteorological dataset from a mid-altitude mountain
617 site (Col de Porte, France, 1325 m alt.) for driving and evaluating snowpack models.
618 *Earth Syst. Sci. Data*, **4**, 13–21, doi:10.5194/essdd-5-29-2012.
- 619

- 620 Oleson, K. W., and Coauthors, 2008: Improvements to the Community Land Model and
621 their impact on the hydrological cycle. *J. Geophys. Res.*, **113**, G01021,
622 doi:10.1029/2007JG000563
623
- 624 Pomeroy, J. W., D. M. Gray, K. R. Shook, B. Toth, R. L. H. Essery, A. Pietroniro, and N.
625 Hedstrom, 1998: An evaluation of snow accumulation and ablation processes for land
626 surface modelling. *Hydrol. Process.*, **12**, 2339–2367, doi:10.1002/(SICI)1099-
627 1085(199812)12:15<2339::AID-HYP800>3.0.CO;2-L.
628
- 629 ———, and E. Brun, 2001: Physical properties of snow. *Snow ecology*, Cambridge
630 University Press Cambridge, 45–126.
631
- 632 Raleigh, M. S., C. C. Landry, M. Hayashi, W. L. Quinton, and J. D. Lundquist, 2013:
633 Approximating snow surface temperature from standard temperature and humidity data:
634 New possibilities for snow model and remote sensing evaluation. *Water Resour. Res.*, **49**,
635 8053–8069, doi:10.1002/2013WR013958.
636
- 637 Rutter, N., and Coauthors, 2009: Evaluation of forest snow processes models
638 (SnowMIP2). *J. Geophys. Res.*, **114**, D06111, doi:10.1029/2008JD011063.
639
- 640 Schirmer, M., and B. Jamieson, 2014: Limitations of using a thermal imager for snow pit
641 temperatures. *Cryosph.*, **8**, 387–394, doi:10.5194/tc-8-387-2014.
642

- 643 Sicart, J. E., 2005: Atmospheric controls of the heat balance of Zongo Glacier (16°S,
644 Bolivia). *J. Geophys. Res.*, **110**, D12106, doi:10.1029/2004JD005732.
- 645
- 646 Singh, R. P., and T. Y. Gan, 2005: Modelling snowpack surface temperature in the
647 Canadian Prairies using simplified heat flow models. *Hydrol. Process.*, **19**, 3481–3500,
648 doi:10.1002/hyp.5839.
- 649
- 650 Slater, A. G., and Coauthors, 2001: The Representation of Snow in Land Surface
651 Schemes: Results from PILPS 2(d). *J. Hydrometeorol.*, **2**, 7–25, doi:10.1175/1525-
652 7541(2001)002<0007:TROSIL>2.0.CO;2.
- 653
- 654 Stössel, F., M. Guala, C. Fierz, C. Manes, and M. Lehning. 2010: Micrometeorological
655 and morphological observations of surface hoar dynamics on a mountain snow cover.
656 *Water Resour. Res.*, **46**, W04511, doi:10.1029/2009WR008198
- 657
- 658 Tarboton, D. G. and C.H. Luce: 1996, Utah Energy Balance Snow Accumulation and
659 Melt Model (UEB) Computer Model Technical Description and Users Guide, *Technical*
660 *report*, Utah State University.
- 661
- 662 Verseghy, D. L., 1991: Class - A Canadian land surface scheme for GCMS. I. Soil model.
663 *Int. J. Climatol.*, **11**, 111–133, doi:10.1002/joc.3370110202.
- 664

665 ———, N. A. McFarlane, and M. Lazare, 1993: Class - A Canadian land surface scheme
666 for GCMS, II. Vegetation model and coupled runs. *Int. J. Climatol.*, **13**, 347–370,
667 doi:10.1002/joc.3370130402.

668

669 Vionnet, V., E. Brun, S. Morin, A. Boone, S. Faroux, P. Le Moigne, E. Martin, and J.-M.
670 Willemet, 2012: The detailed snowpack scheme Crocus and its implementation in
671 SURFEX v7.2. *Geosci. Model Dev.*, **5**, 773–791, doi:10.5194/gmd-5-773-2012.

672

673 Warren, S. G., and W. J. Wiscombe, 1980: A model for the spectral albedo of snow. II:
674 Snow containing atmospheric aerosols. *J. Atmos. Sci.*, **37**, 2734–2745,

675

676 Wiscombe, W. J., and S. G. Warren, 1980: A model for the spectral albedo of snow. I:
677 Pure snow. *J. Atmos. Sci.*, **37**, 2712–2733,

678

679 **Table 1.** Instrumentation used at various sites

	Snow surface temperature	Wind speed	Temperature and humidity	Short and Long-wave radiation
Pomeroy Acreage, Canada	Exergen IRTC, KZ CNR1	Met One 014A 3-cup	Vaisala HMP45	KZ CNR1
Kernen Farm, Canada	KZ CNR1	Met One 014A 3-cup	Vaisala HMP45	KZ CNR1
Mud Lake, Canada	KZ CNR1	Campbell Scientific CSAT3 sonic	Vaisala HMP45	KZ CNR1
Zongo Glacier, Bolivia	KZ CNR1	RM Young wind monitor	Vaisala HMP45	KZ CNR1
Col du Porte, France	Exergen IRTC, KZ CG4	Laumouier	Vaisala HMP35/45	Epply PIR/ KZ CG4, KZ CM7/14
Hay Meadow, Canada	KZ CNR1	Met One Sonic	Vaisala HMP45	KZ CNR1

680

681

682 **Table 2.** Parameters, biases and rms errors for optimized snow surface temperature
683 simulations.

	Shortwave absorption	Roughness (m)	bias (K)	rms error (K)
Pomeroy	0.05	0.005	0.26	1.20
Col de Porte	0.13	0.063	0.33	2.15
Hay Meadow	0.10	0.008	-0.04	3.13
Kernen	0.10	0.002	0.31	1.27
Mud Lake	0.00	0.001	0.17	0.86
Zongo	0.13	0.032	-0.02	1.22

684

685 **Table 3.** rms errors (K) and bias (K) for simulations with global parameters (0% or 10%
 686 SW absorption, 0.03 m or 0.003 m roughness length). Smallest rms errors and bias are **in**
 687 **bold.** The global parameter sets selected are *italicized*.

	0% SW absorption				10% SW absorption			
	smooth		rough		smooth		rough	
	rms	bias	rms	bias	rms	bias	rms	bias
Pomeroy	1.33	-0.22	1.68	1.01	<i>1.30</i>	<i>0.24</i>	1.78	1.22
Col de Porte	4.22	-2.18	3.32	-0.99	2.94	-1.26	<i>2.31</i>	<i>-0.29</i>
Hay Meadow	4.33	-2.41	3.77	<i>1.33</i>	<i>3.52</i>	<i>-1.35</i>	3.73	1.87
Kernen	1.65	<i>0.16</i>	2.26	1.34	<i>1.33</i>	<i>0.59</i>	2.35	1.60
Mud Lake	<i>1.05</i>	<i>0.65</i>	2.18	1.75	1.18	0.81	2.23	1.82
Zongo	4.74	-3.86	2.14	-0.89	3.08	-2.43	<i>1.29</i>	<i>-0.22</i>

688

689

690

691

692 **Table 4.** rms errors (K) for approximating snow surface temperature by air temperature,
 693 dew point temperature or wet bulb temperature and the increase in rms error (in brackets)
 694 compared with those for the selected global parameters for IPM (selected set is *italicized*
 695 in Table 3).

	Ta	Td	Tw
Pomeroy	3.87 (2.57)	3.00 (1.7)	3.27 (1.97)
Col de Porte	6.91 (4.6)	4.57 (2.26)	5.63 (3.32)
Hay Meadow	9.85 (6.33)	7.23 (3.71)	7.61 (4.09)
Kernan	3.96 (2.63)	3.52 (2.19)	3.82 (2.49)
Mud Lake	4.72 (3.67)	2.20 (1.15)	3.10 (2.05)
Zongo	6.63 (5.34)	6.28 (4.99)	2.56 (1.27)

696

697

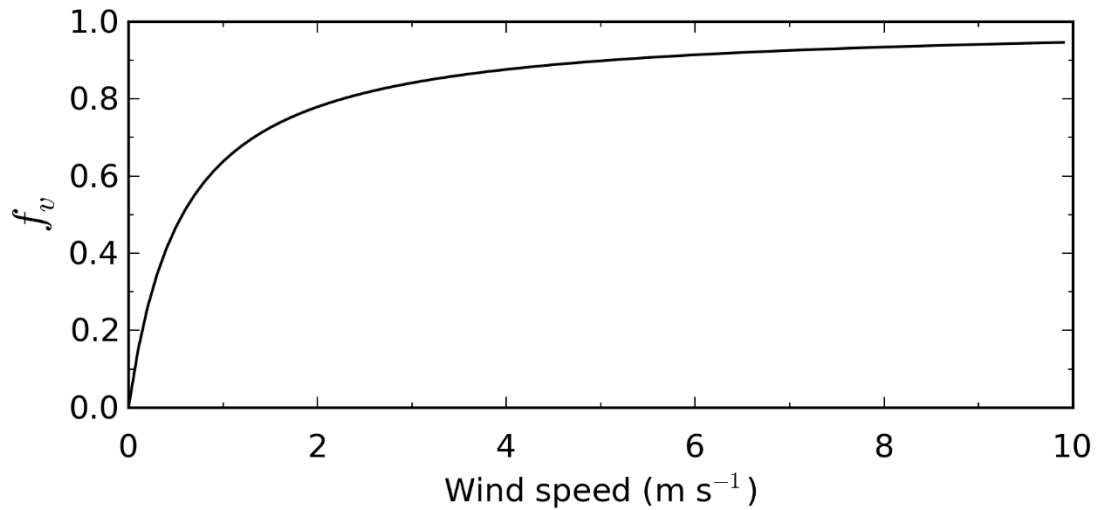
698 **FIGURES**

699

700 **Figure 1.** A snowpack surface cross-sectional photograph taken in April 2003 in Wolf
701 Creek Research Basin, Yukon Territory, Canada. The cold snowpack has poorly bonded
702 surface crystals and displays light penetration indicative of its porous medium nature.

703

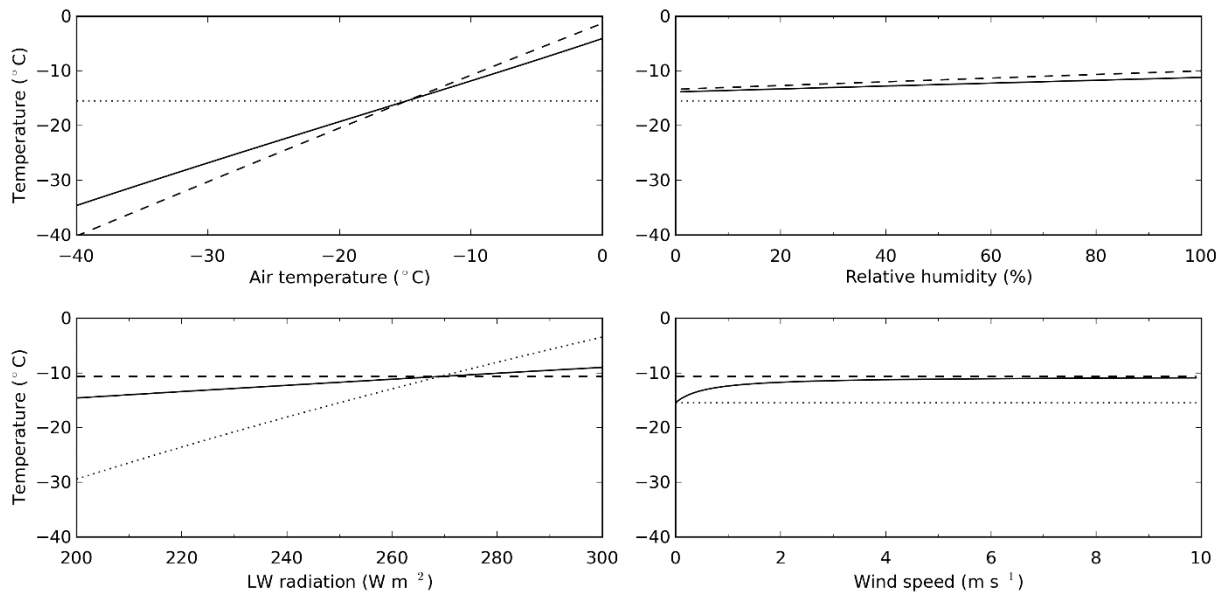
704



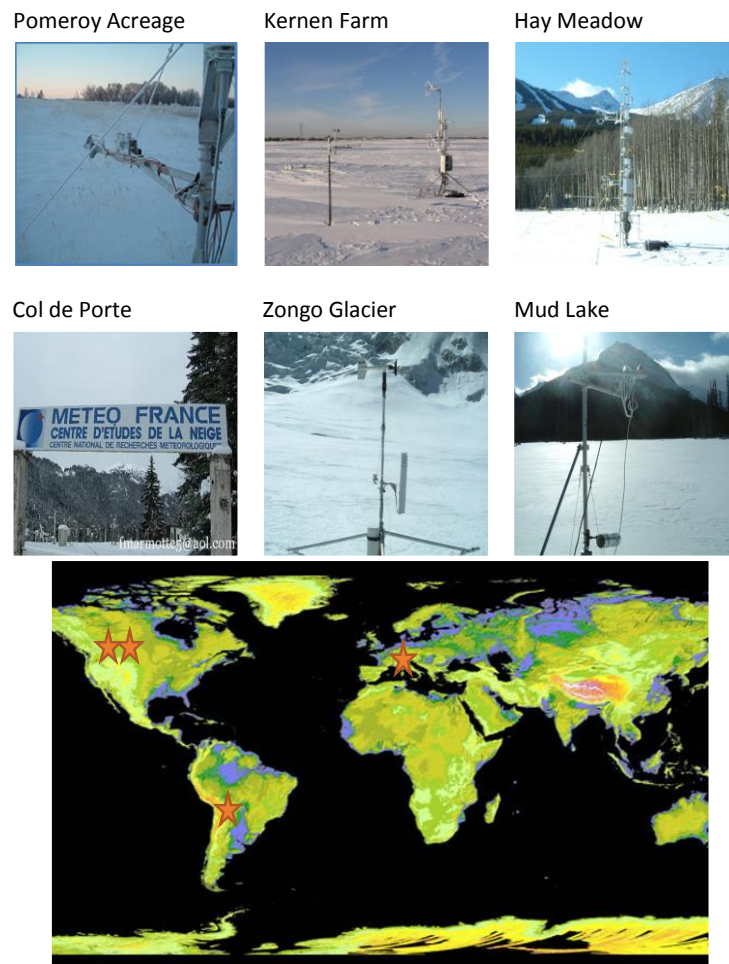
705 **Figure 2.** Sensitivity of the ventilation factor, f_v , to wind speed for air temperature of -
706 10°C, relative humidity of 80%, no incoming shortwave radiation, incoming longwave
707 radiation of 250 W m⁻² and aerodynamic roughness length of 3×10^{-3} m. Reference height
708 for atmospheric variables is 2 m above the snow surface.

709

710



711 **Figure 3.** Sensitivity of simulated SST (solid line), aerodynamic equilibrium
 712 temperature (dashed line) and radiative equilibrium temperature (dotted line) to variations
 713 in air temperature, relative humidity, incoming longwave radiation and wind speed for an
 714 aerodynamic roughness length of 3×10^{-3} m and no incoming shortwave radiation.
 715 Reference heights for atmospheric variables are 2 m above the snow surface. As each
 716 variable is changed, the others are kept fixed at an air temperature of -10°C , relative
 717 humidity of 80%, incoming longwave radiation of 250 W m^{-2} and wind speed of 2 m s^{-1} .
 718

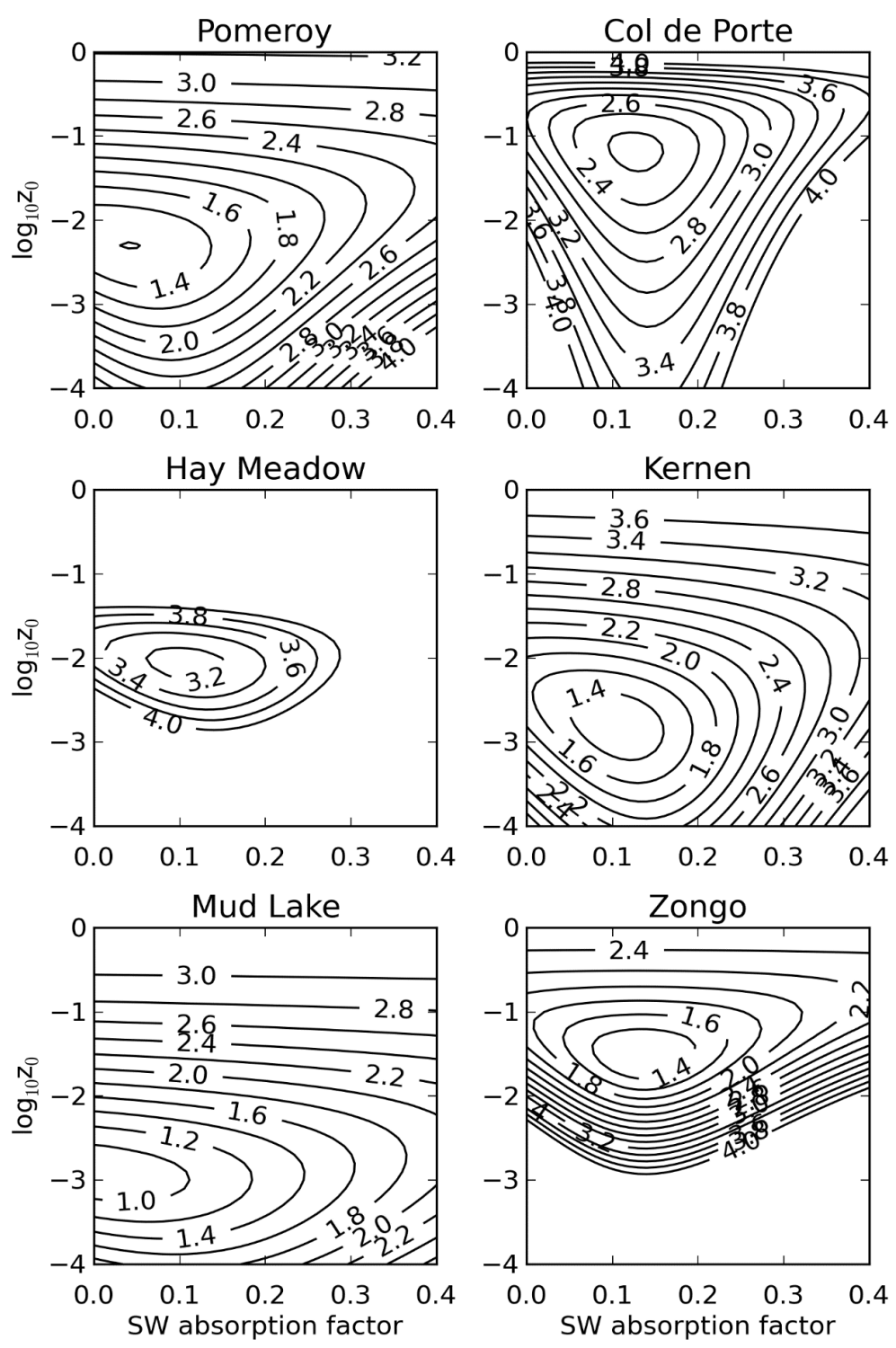


719

720

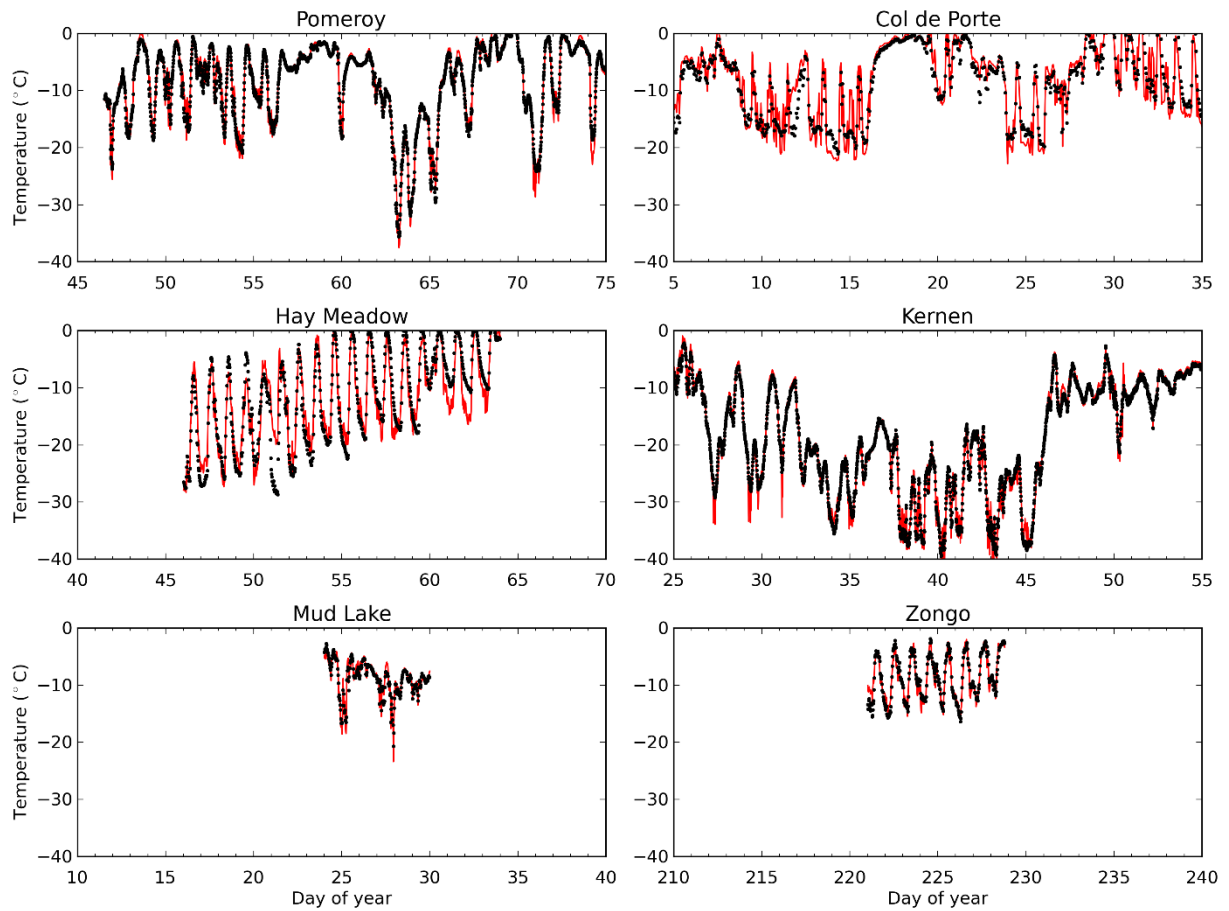
721 **Figure 4.** Location of field sites and site photographs.

722



723
724 **Figure 5.** Sensitivity of model rms error (contour interval 0.2°C) to variations in shortwave
725 radiation absorption and aerodynamic roughness parameters.

726

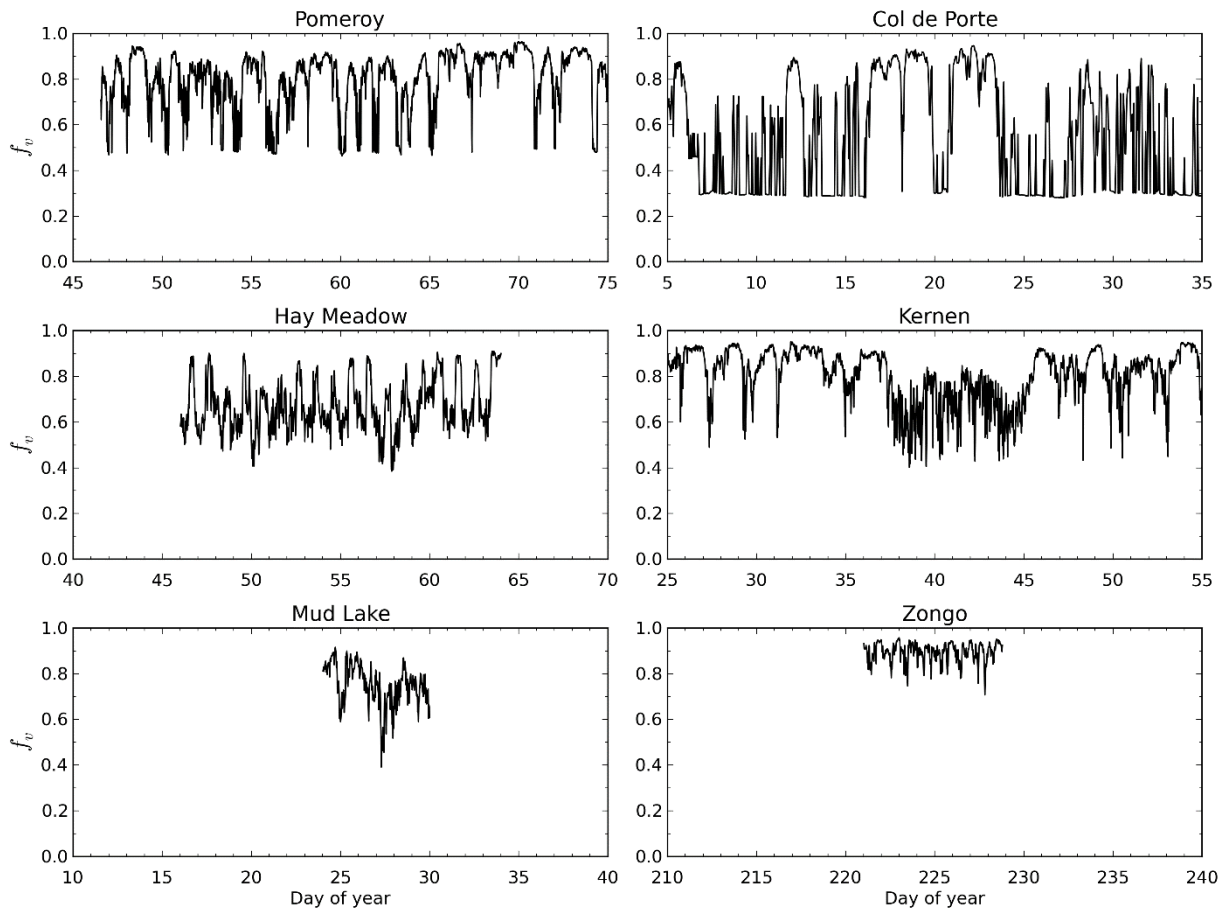


727

728 **Figure 6.** SST measured (black dots) and modelled (red lines) with RPM at the six sites

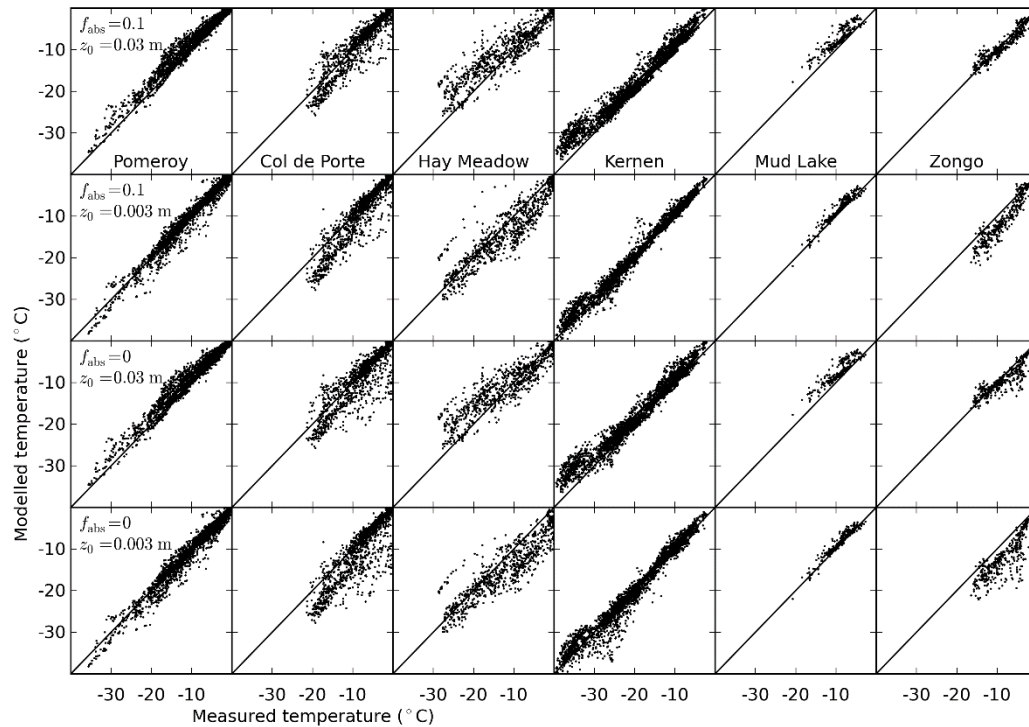
729 using optimized parameters from Table 2.

730



731
732
733

Figure 7. Ventilation factor, f_v , at the six sites as calculated using the RPM.



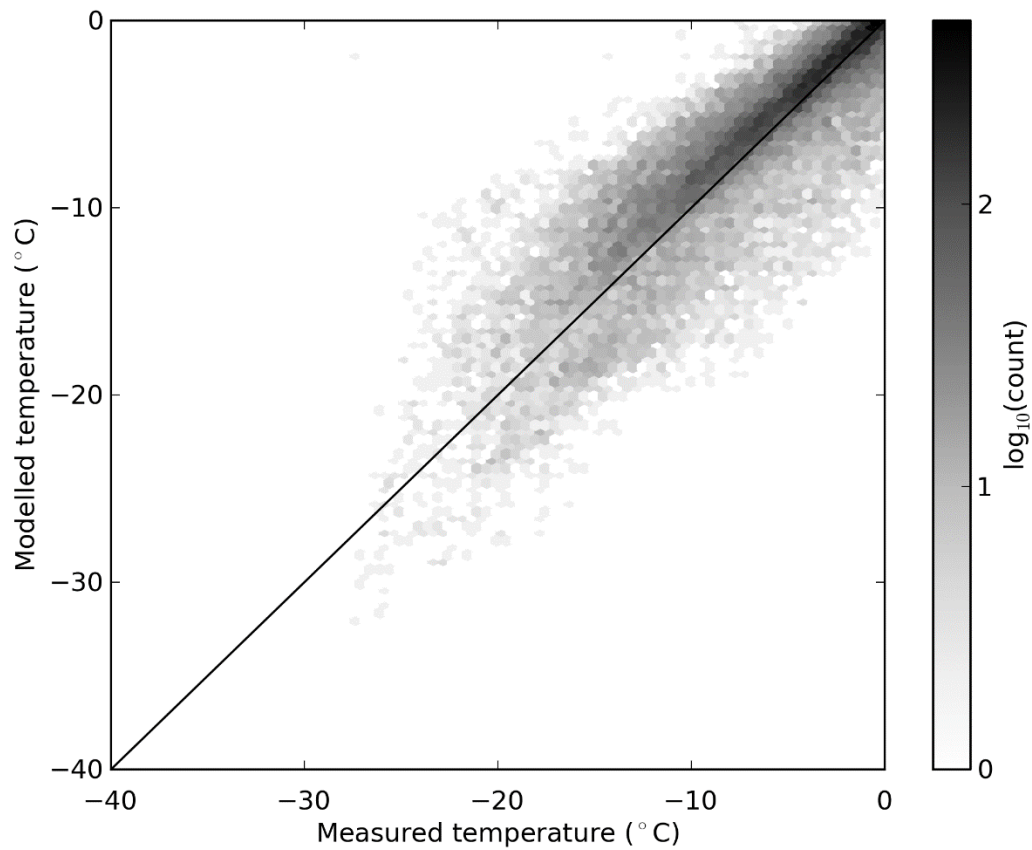
734

735

736 **Figure 8.** Scatterplot of measured and RPM simulated SST for the six sites with four sets

737 of global parameters, (0% or 10% SW absorption, 0.03 m or 0.003 m roughness length).

738



739

740 **Figure 9.** Scatter plot using tonal density to show the number of points in small hexagons

741 representing measured and modelled SST for Col de Porte over 18 years using the

742 shortwave absorption factor of 0.1 and aerodynamic roughness height of 0.03 m.

743

744